Current Biology 23, 569–574, April 8, 2013 ©2013 Elsevier Ltd All rights reserved http://dx.doi.org/10.1016/j.cub.2013.02.026

Report

Keratocyte Fragments and Cells Utilize Competing Pathways to Move in Opposite Directions in an Electric Field

Yaohui Sun,[1,2,3] Hao Do,[1] Jing Gao,[1,5] Ren Zhao,[1,6] Min Zhao,[1,4,*] and Alex Mogilner[2,3,*]
[1]Institute for Regenerative Cures, Department of Dermatology, and Department of Ophthalmology, University of California Davis School of Medicine, Sacramento, CA 95817, USA
[2]Department of Neurobiology, Physiology, and Behavior
[3]Department of Mathematics
[4]Center for Neuroscience
University of California, Davis, Davis, CA, 95616, USA
[5]Yunnan Normal University, Kunming, Yunnan 650092, China
[6]Department of Orthopedics, Daping Hospital, Third Military Medical University, Chongqing 400042, China

Summary

Sensing of an electric field (EF) by cells—galvanotaxis—is important in wound healing [1], development [2], cell division, nerve growth, and angiogenesis [3]. Different cell types migrate in opposite directions in EFs [4], and the same cell can switch the directionality depending on conditions [5]. A tug-of-war mechanism between multiple signaling pathways [6] can direct *Dictyostelium* cells to either cathode or anode. Mechanics of motility is simplest in fish keratocytes, so we turned to keratocytes to investigate their migration in EFs. Keratocytes sense electric fields and migrate to the cathode [7, 8]. Keratocyte fragments [9, 10] are the simplest motile units. Cell fragments from leukocytes are able to respond to chemotactic signals [11], but whether cell fragments are galvanotactic was unknown. We found that keratocyte fragments are the smallest motile electric field-sensing unit: they migrate to the anode, in the opposite direction of whole cells. Myosin II was essential for the direction sensing of fragments but not for parental cells, while PI3 kinase was essential for the direction sensing of whole cells but not for fragments. Thus, two signal transduction pathways, one depending on PI3K, another on myosin, compete to orient motile cells in the electric field. Galvanotaxis is not due to EF force and does not depend on cell or fragment size. We propose a "compass" model according to which protrusive and contractile actomyosin networks self-polarize to the front and rear of the motile cell, respectively, and the electric signal orients both networks toward cathode with different strengths.

Results and Discussion

Cells and Their Fragments Migrate in Opposite Directions in an EF

Keratocytes, as well as other motile cell types [12], can spontaneously detach cell fragments that move with shapes, speeds, and persistence similar to those of whole cells [9, 10]. Both fragments and parental cells cultured without application of an electric field (EF) showed migration in random directions, with a directedness value close to zero (Figures 1C and 1D). When exposed to EFs, both cells and fragments, which are devoid of nuclei and major organelles (Figure S1 available online), migrated directionally. Surprisingly, the cell fragments migrated to the anode, while the parental cells migrated to the cathode (Figure 1, Movie S1, and Movie S2).

This directional migration was further confirmed with multiple reversal of the EF polarity, which induced rapid reversal of the migration direction every time in both fragments and cells (Figure S2). Starting from an EF strength of 0.5 V/cm, increase of EFs increased directedness for both cells and fragments (Table S1). The speed of cells, but not of fragments, increased moderately with the EF strength (Figure 1D).

The shapes of cells and fragments before EF application were not changed significantly by EFs (Figures S3A and S3B). For keratocyte cells [13] and fragments [10], it has been shown that quantitative changes in the principal modes of variations of cell shape are indicators of changes in the self-organization of the actin-myosin networks and consequent changes in biophysical motile machinery. Thus, the EF invariance of the shapes of fragments and cells indicates that an EF mainly orients fragments and cells without affecting organization of the actin-myosin networks. To assess the role of actin dynamics in EF sensing, we used the Arp2/3 inhibitor CK-666. Both perturbed cells and fragments slowed down significantly, yet remained strongly directional, to cathode and anode, respectively (Figure 2 and Table S1). Thus, actin machinery itself is unlikely to be a part of the signaling transduction pathway of galvanotaxis.

PI3K Inhibition Does Not Affect Fragments, but Reverses Cells to the Anode

What could be the mechanisms for fragments to migrate oppositely to their parental cells? In neutrophils, two antagonistic pathways—"frontness" and "backness"—were proposed to segregate the actin-protruding and actin-myosin contractile networks to the front and rear, respectively, and to orient the front up the chemotactic gradient [14]. When Rac was inhibited and the frontness pathway weakened, the cell rear oriented up the chemotactic gradient, and cell migration shifted down the gradient. Though galvanotaxis has a different sensor, it shares known signal transduction pathways and molecules with chemotaxis (PI3Ks, PIP2/PIP3, and PTEN in *Dictyostelium* [15] and microtubules and Rho GTPases in nerve growth cones [16]).

We hypothesized that, similarly, two pathways—frontness and backness—compete to orient cells in EFs in opposite directions, and that the frontness is stronger than the backness in cells, with the opposite being true in fragments. This hypothesis predicts that if the frontness is weakened, the cells in an EF would reorient from the cathode to the anode by the previously overwhelmed backness. On the other hand, the fragments' directionality should not be affected because in them the backness dominates, and weakening of the frontness would not change this balance.

PI3 kinase is a key part of direction-sensing frontness pathways relaying signals to actin [17]; therefore, we tested

*Correspondence: minzhao@ucdavis.edu (M.Z.), mogilner@math.ucdavis.edu (A.M.)

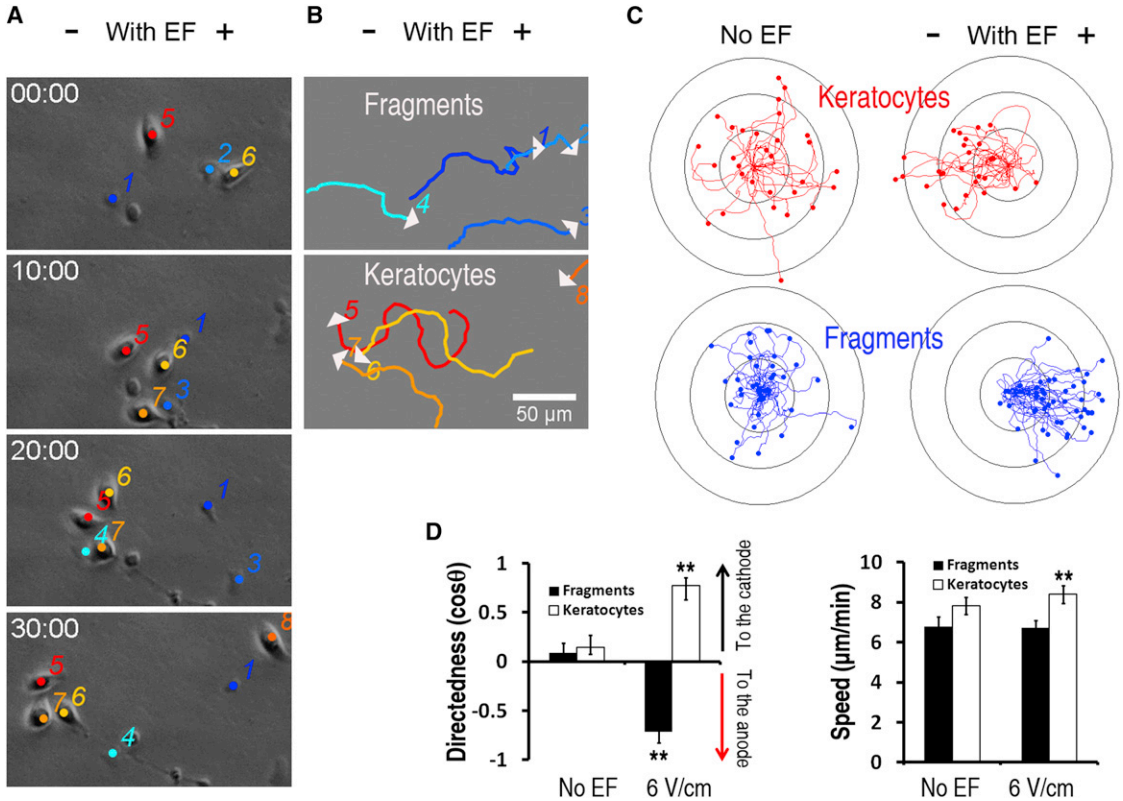

Figure 1. EFs Direct Migration of Fragments to the Anode, in the Opposite Direction of that of the Parental Keratocytes

(A) Fragments (1 to 4) migrate to the anode in EFs, in an opposite direction of their parental keratocytes (5 to 8). Time is in min:s. The scale bar represents 50 μm.

(B and C) Migration trajectories over 30 min of keratocytes (red in C) and fragments (blue in C) in the presence or absence of EFs with polarity as shown. White arrows indicate migration direction in (B).

(D) Directedness and trajectory speed of fragments and keratocytes. Data are shown as means ± SEM. See Figure S2 and Table S1 for related data. **$p < 0.01$ when compared to the control in the absence of an EF.

EF = 6 V/cm. Ring unit, 100 μm; duration, 30 min. See also Figure S2, Table S1, Movie S1, and Movie S2.

whether PI3K influences the migration direction of keratocytes and fragments. PI3K inhibition with LY294002, in agreement with our hypothesis, switched the directional migration of cells from the cathode to the anode (Figure 2). Although the overall number of motile cells and cell speed were decreased by this perturbation, a great fraction of keratocytes maintained persistent motility (Figure S4A). As can be seen clearly in stronger EFs (Figure S4B), the majority of cells migrate to the anode, but a few cells maintain the cathodal migration. As expected, LY294002 did not have significant effects on the anode-directed migration of fragments (Figure 2).

Myosin Inhibition Disrupts Directional Sensing of Fragments but Not Cells

According to our hypothesis, weakening of the backness should reorient the fragments from the anode to the cathode, but not the cells' cathodal migration. We tested the effect of myosin inhibition, because myosin is associated with controlling the motile cell rear. Indeed, blebbistatin, a small-molecule inhibitor of myosin, did not affect the directional cell migration (Figure 2). However, rather than reorienting the fragments, blebbistatin treatment abolished the anode directed migration of fragments (Figure 2). Interestingly, fragments did not migrate in completely random direction: a statistically significant majority of the myosin-inhibited fragments in EFs migrated along the EF direction, to either the anode or the cathode (Figure 2B). We used another compound, Y27632, to inhibit the Rho-associated kinase (ROCK) and myosin downstream. ROCK inhibition abolished directional migration of fragments to the anode but had little effects on cathode directed migration of cells (Figure 2).

To investigate whether the signal transduction was limited to the PI3K- and myosin-mediated pathways, we applied LY294002 and blebbistatin simultaneously. When both pathways were inhibited, directionality of both cells and fragments in EFs was lost completely (Figure 2 and Table S1). Moreover, there was no longer a bias to the quadrants represented by either the cathode or anode as opposed to the up or down quadrants. Therefore, a parallel independent pathway transducing the EF signal is unlikely.

Depletion of Extracellular Calcium Disrupts Directional Sensing of Fragments but Not Cells

We then asked what could be the basis for different relative strengths of the frontness and backness pathways in cells and fragments and investigated possible regulators upstream of myosin. The fragments are devoid of endoplasmic reticulum (Figure S1), the major store of intracellular Ca^{2+}, which could alter Ca^{2+} dynamics in fragments. Ca^{2+} channels are involved in keratinocytes' galvanotaxis [18] and are proposed to regulate keratocytes' response to EFs [7]. Varying extracellular Ca^{2+} affects the direction of granulocyte migration in EFs [5].

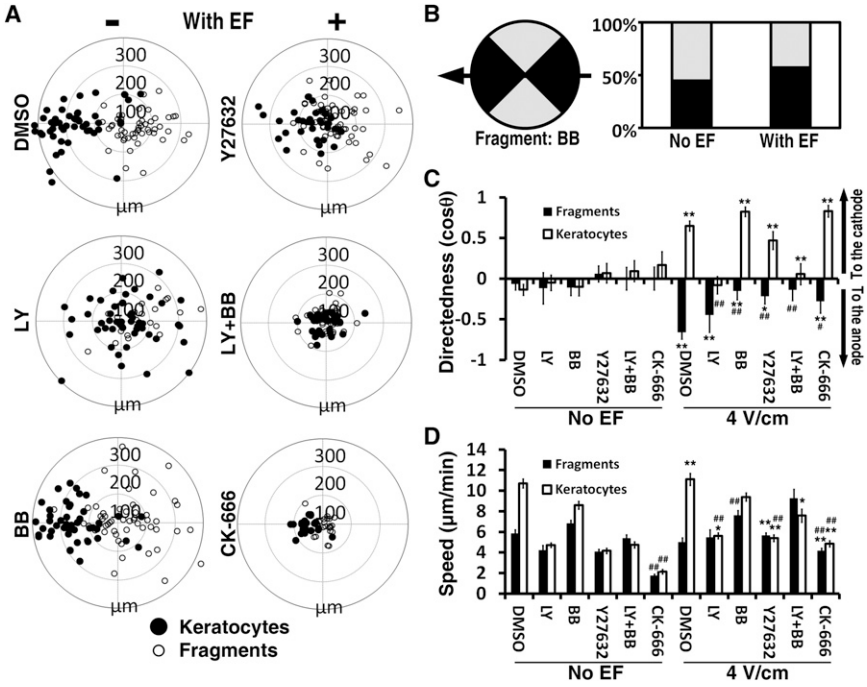

Figure 2. Distinctive Roles for Myosin and PI3K Signaling in Cells and Fragments in Determination of EF-Guided Migration Direction

(A) Trajectories' end points (after 30 min migration) of keratocytes (black circles) and fragments (white circles). PI3 kinase inhibition (LY) biases cells' directionally in parallel to the EF vector, with the majority of cells going to the anode, although many cells still migrate to the cathode, and had no effects on directional migration of fragments. Inhibition of myosin (BB and Y27632) abolished directional migration of fragments but had no significant effects on keratocytes. Double inhibition of PI3K and myosin (LY+BB) rendered both cells and fragments nondirectional. Inhibition of Arp2/3 (CK-666) slowed down both cells and fragments but did not cancel their respective directionalities.

(B) EF biases fragments' directionally in parallel to the EF vector (arrow) in the presence of myosin inhibitor. The percentage of the fragments in horizontal quadrants (dark) was increased upon EF stimulation. The differences between the no-EF and EF groups are significant ($p < 0.01$).

(C and D) Directedness (C) and trajectory speed (D) of fragments and keratocytes in (A). * ($p < 0.05$) and ** ($p < 0.01$) indicate that the difference between no EF and an EF is significant. ## ($p < 0.01$) indicates that the difference between drug treatment and DMSO vector control is significant. Data are shown as means ± SEM.

EF = 4 V/cm. Ring unit, 100 μm; duration, 30 min. See also Figure S4 and Table S1.

We used EGTA, a chelating agent, to deplete extracellular Ca^{2+}. In addition to lowering the average speeds of cells and fragments, this perturbation rendered fragments nondirectional in EFs (Figures 3A and 3B). Because myosin and adhesion turnover are regulated through Ca^{2+} [19], one possibility is that due to different Ca^{2+} regulation in cells and fragments, myosin and adhesion strengths and distributions are affected differently, leading to different transduction of the galvanotactic signals along two pathways in cells and fragments.

Perturbation of Microtubules Has No Effect on Cell and Fragment Galvanotaxis

Another difference between the cells and fragments is the presence of microtubules in the former and absence in the latter [20]. Microtubules do not affect keratocyte cell motility [13], and disruption of microtubules does not affect keratocytes' galvanotaxis [10]. Disruption of microtubules with nocodazole did not affect the directedness of either cells or fragments in EFs (Figure 3C). Thus, different microtubule-mediated signaling is not the cause of the different balance of the anode- and cathode-directing pathways of galvanotaxis.

Directional Sensing Does Not Depend on Cell or Fragment Sizes

Yet another difference between the cells and fragments is their size, with cells having four times greater surface area than fragments (Figure S3C). This could potentially lead to differences in both initial EF-sensing mechanisms (the effect of the membrane potential gradient is proportional to both the cell size and EF strength [21]) and signal transduction (i.e., reaction-diffusion-based sensing depends on proper scaling of chemical concentrations with size [22]). However, neither cell nor fragment directedness depends on their sizes, while the directedness of both depends on the EF strength (Figure S3C). In fact, the smaller fragments are more sensitive to weaker EFs (~0.5 V/cm) than the larger cells (~1 V/cm) (Table S1).

The Galvanotactic Effect Is Not the Result of Direct Electric Force Sensing

In principle, if the cell and fragment bear opposite surface charges, the electrostatic and osmotic forces on their surfaces in EF would be opposite [23]. However, in suspension, both cells and fragments are dragged to the cathode with similar speeds in EFs (Figure S3D), so their surfaces have charges of the same sign and similar density, and the electric forces would drag them in the same direction.

Another serendipitous observation argues against the direct force-sensing: often, fragments stay connected to mother cells by membrane tethers. (The diffusion of signaling molecules through the tether is much slower than the characteristic migration time scale [24], so the mother cell and fragment do not share signaling pathways.) In this state, cell or fragment pairs often moved in opposite directions (cathode or anode, respectively) for minutes, until the tether was stretched up to tens of microns (Figure 4 and Movie S3), at which point both cell and fragment were stalled. When PI3K was inhibited, both cell and fragment connected by the tether migrated to anode, but the cell was usually faster and would outrun the fragment, after which the cell and fragment in its wake traveled together without stretching the tether further (Figure 4). When myosin was inhibited, the cathode-directed cell rapidly left the fragment behind, stretching the tether sometime by more than 100 μm (Figures 4A and 4B). This indicates that cells and fragments are unlikely to respond to mechanical force exerted by EFs on charged cells, because such force of at

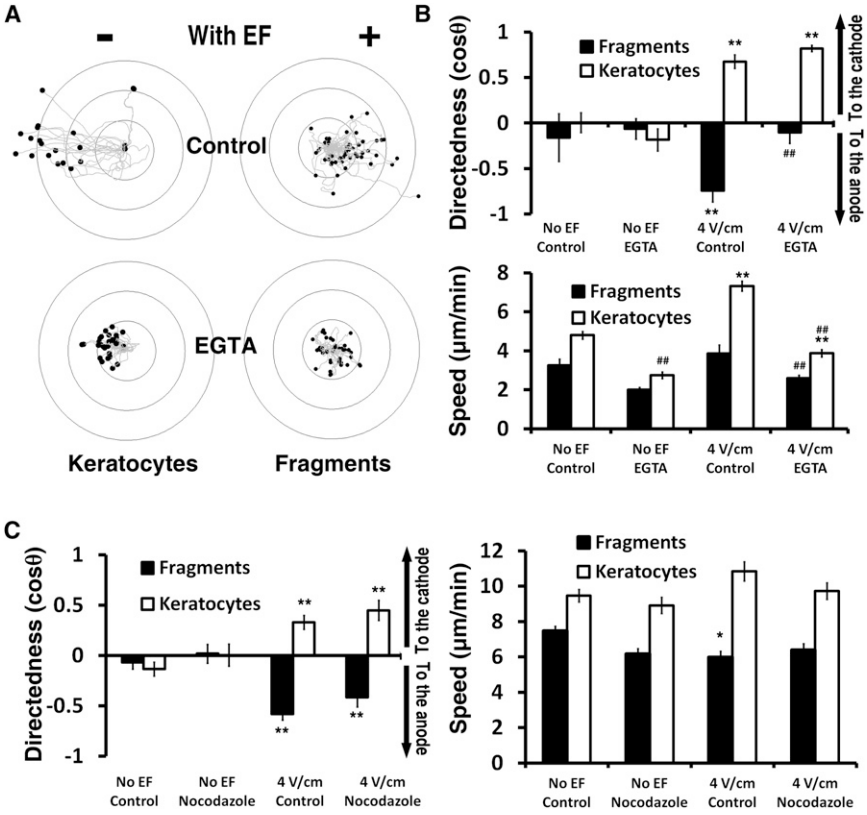

Figure 3. Calcium Signaling Is Required for Galvanotaxis of Fragments but Not Cells, Whereas Microtubules Are Dispensable for Both

(A) EGTA (5 mM) abolished the directional migration of fragments, but not that of keratocytes. Migration speed decreased significantly in both the fragments and keratocytes.

(B) Quantification of directionality and speed of keratocytes and fragments with or without Ca^{2+} depletion. EGTA impairs fragment directionality and slows down both cell and fragment migration. **p < 0.01 when compared to no EF control; ##p < 0.01 when compared to that in EF without treatment of EGTA.

(C) Directionality and speed of keratocytes and fragments in the presence and absence of Nocodazole. * (p < 0.05) and ** (p < 0.01) indicate that the difference between no EF and EF is significant. ## (p < 0.01) indicates that the difference between Nocodazole and DMSO vector control is significant.

EF = 4 V/cm. Ring unit, 100 μm; duration, 30 min. In (B) and (C), data are shown as means ± SEM. See also Figure S1 and Table S1.

most 10 pN [23] would be overwhelmed by the opposite tether force of tens of piconewtons. The EF signal orients the tethered cell and fragment effectively enough for the cell and fragment to persist despite the opposing mechanical forces.

Finally, we tested how the cell and fragment directedness depended on external pH and found that, in agreement with [23], the cells maintained the cathodal-oriented motility in the wide range of pH only losing the directedness at pH < 6 (Figure S4C). Interestingly, the fragments sensed EFs in the range of pH similar to that of the EF-sensing cells (Figure S4C), pointing indirectly to the same physical EF sensor in the cells and fragments.

"Compass" Model of Galvanotaxis

We conclude that the cell fragment—the simplest and smallest cell migration unit—is also the smallest EF-sensing unit, containing both the EF sensor and the relevant signal transduction pathways. These PI3K- and myosin-dependent pathways perform differently in cells and fragments. We propose that two competing pathways direct cells in an EF (see the graphical abstract available online): a PI3K-dependent pathway signaling to the protruding actin network at the cell front, orienting the front toward cathode, and a myosin-dependent pathway signaling to the contractile actin-myosin network at the cell rear, orienting the rear also toward the cathode. The PI3K-dependent pathway dominates in cells, while the myosin-dependent pathway dominates in fragments. In the whole cell, the signal orienting the protruding actin network toward the cathode is stronger, so the cell front is facing the cathode. In the fragment, the signal orienting the contractile actin-myosin network at the rear toward the cathode is stronger, so the fragment rear is facing the cathode and the front is facing the anode.

The identity of the factors that govern these two pathways differently in cells and fragments remains unknown. One possibility could stem from different PIP3/PTEN or other activator/inhibitor ratios in cells and fragments. Another is that fragments' ability to regulate intracellular Ca^{2+} levels is diminished, so EF could create a Ca^{2+} gradient in a fragment but not in a whole cell, rendering myosin-related signaling at the fragment rear relatively stronger. No long-lasting Ca^{2+} gradient within the keratocyte cell lamellipodium has been observed [8, 23], so it is likely that in whole cells Ca^{2+} is buffered and does not develop spatial gradients. Yet another possibility is that, mechanically, myosin could have a weaker steering effect on the whole cells than on fragments. Related to that, fragments are unlikely to inherit much myosin from mother cells; the myosin that they inherit is weakened and does not affect the motility mechanics [10, 24], so the fact that myosin-mediated steering in EFs is crucial is puzzling. Perhaps a signaling, not mechanical, function of myosin is essential for the EF sensing. Our data argue against involvement of the actin assembly dynamics in the galvanotaxis, but whether all actin networks are only downstream readouts of signaling pathways, unlike in neutrophils [25], requires further investigation.

Many studies have gradually converged on a number of hypotheses about how cells can sense EFs. First, an EF induces a gradient in the membrane electric potential [21], which can affect asymmetrically ion fluxes that could signal to the motile machinery. Second, cells are oriented by fluid flow [8], and the EF creates an electro-osmotic flow near the charged plasma membrane. Third, charged signaling proteins in the plasma membrane can be dragged by an electric force aggregating at one cell edge [26] and spatially biasing the signaling. Fourth, the cell can feel the force of an EF on the charged proteins in the plasma membrane. Following [23], our data suggest that electro-osmosis is unlikely to be the factor triggering galvanotaxis: since cells and fragments have similar surface charges and very different shapes, the electro-osmotic flow should pull both cell and fragment in

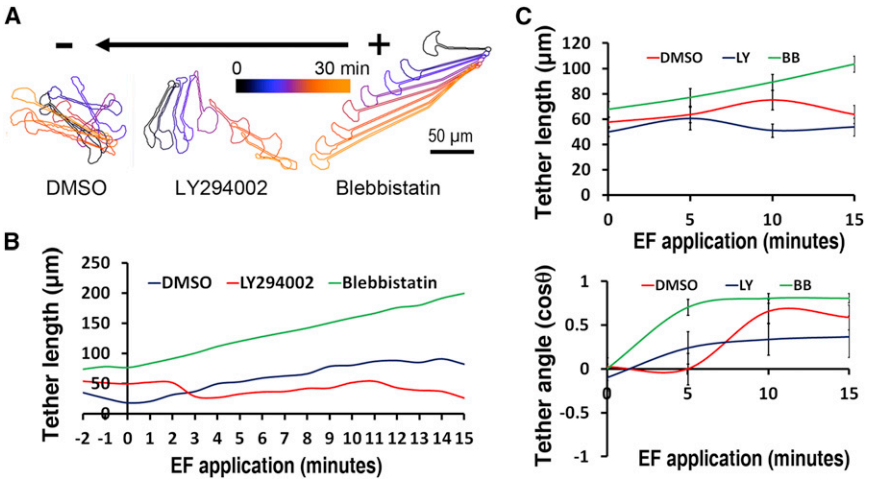

Figure 4. Galvanotaxis of Fragments Tethered to Mother Cells

(A) Migration of tethered fragments and cells in the presence of DMSO (left), LY294002 (middle) or Blebbistatin (right), in an EF of 4 V/cm in the indicated orientation. The overlaid contours of different time point after EF application are color coded. The scale bar represents 50 μm.

(B) Typical scatter plots of tether lengths in the presence of blebbistatin (green line, increasing length) and LY294002 (red line, decreasing length) when compared to DMSO (blue line, increasing length).

(C) Quantification of average tether lengths and tether angles after EF exposure in the presence of blebbistatin (green line) and LY294002 (red line) when compared to DMSO (blue line). Note that the average direction of the tether in the control case does not change for a while because initially the cell and fragment pass each other side by side in the opposite directions, and the tether simply rotates. After that, the cell is closer to the cathode and the fragment is closer to the anode, and their further divergence orients the tether along the EF. In the case of the perturbations, the tether is oriented by the leading cell much faster. Data are shown as means ± SEM.

See also Figure S3 and Movie S3.

the same direction, and the effect of fluid flow on the great mound of the cell body would be different from that on the flat and small fragment. The observation that a mechanical opposing force could not reorient cells and fragments suggests that direct electric force sensing is unlikely to be the galvanotactic mechanism. Our data agree with the hypothesis that electrophoresis of charged membrane proteins could be the initial signal of galvanotaxis in the keratocytes [23], as cells and fragments maintain their directedness in EF in similar ranges of pH (loss of the signal in acidic medium likely indicates that protonation of some charged proteins on the cell surface abolishes their drift in EFs). This also hints at the same upstream EF sensor in cells and fragments.

Supplemental Information

Supplemental Information includes four figures, one table, Supplemental Experimental Procedures, and three movies and can be found with this article online at http://dx.doi.org/10.1016/j.cub.2013.02.026.

Acknowledgments

We are grateful to Greg Allen, Orion Weiner, and Roy Wollman for fruitful discussions, useful suggestions, and critical reading of this manuscript. We thank Noa Ofer and Kinneret Keren for sharing endoplasmic reticulum images. This work was supported by National Institutes of Health grants GM068952 to A.M. and 1R01EY019101 to M.Z., as well as by California Institute of Regenerative Medicine Research grant RB1-01417 and National Science Foundation Grant MCB-0951199 to M.Z and P. Devreotes, whose support we gratefully acknowledge.

Received: August 2, 2012
Revised: January 4, 2013
Accepted: February 11, 2013
Published: March 28, 2013

References

1. Huttenlocher, A., and Horwitz, A.R. (2007). Wound healing with electric potential. N. Engl. J. Med. *356*, 303–304.
2. Levin, M., Thorlin, T., Robinson, K.R., Nogi, T., and Mercola, M. (2002). Asymmetries in H+/K+-ATPase and cell membrane potentials comprise a very early step in left-right patterning. Cell *111*, 77–89.
3. Zhao, M. (2009). Electrical fields in wound healing-An overriding signal that directs cell migration. Semin. Cell Dev. Biol. *20*, 674–682.
4. Guo, A., Song, B., Reid, B., Gu, Y., Forrester, J.V., Jahoda, C.A., and Zhao, M. (2010). Effects of physiological electric fields on migration of human dermal fibroblasts. J. Invest. Dermatol. *130*, 2320–2327.
5. Franke, K., and Gruler, H. (1990). Galvanotaxis of human granulocytes: electric field jump studies. Eur. Biophys. J. *18*, 335–346.
6. Sato, M.J., Kuwayama, H., van Egmond, W.N., Takayama, A.L., Takagi, H., van Haastert, P.J., Yanagida, T., and Ueda, M. (2009). Switching direction in electric-signal-induced cell migration by cyclic guanosine monophosphate and phosphatidylinositol signaling. Proc. Natl. Acad. Sci. USA *106*, 6667–6672.
7. Cooper, M.S., and Schliwa, M. (1986). Motility of cultured fish epidermal cells in the presence and absence of direct current electric fields. J. Cell Biol. *102*, 1384–1399.
8. Huang, L., Cormie, P., Messerli, M.A., and Robinson, K.R. (2009). The involvement of Ca2+ and integrins in directional responses of zebrafish keratocytes to electric fields. J. Cell. Physiol. *219*, 162–172.
9. Verkhovsky, A.B., Svitkina, T.M., and Borisy, G.G. (1999). Self-polarization and directional motility of cytoplasm. Curr. Biol. *9*, 11–20.
10. Ofer, N., Mogilner, A., and Keren, K. (2011). Actin disassembly clock determines shape and speed of lamellipodial fragments. Proc. Natl. Acad. Sci. USA *108*, 20394–20399.
11. Malawista, S.E., and de Boisfleury-Chevance, A. (1991). Cryopreserved cytoplasts from human polymorphonuclear leukocytes (cytokineplasts) are chemotactic at speeds comparable to those of fresh intact cells. J. Leukoc. Biol. *50*, 313–315.
12. Keller, H.U., and Bessis, M. (1975). Migration and chemotaxis of anucleate cytoplasmic leukocyte fragments. Nature *258*, 723–724.
13. Keren, K., Pincus, Z., Allen, G.M., Barnhart, E.L., Marriott, G., Mogilner, A., and Theriot, J.A. (2008). Mechanism of shape determination in motile cells. Nature *453*, 475–480.
14. Xu, J., Wang, F., Van Keymeulen, A., Herzmark, P., Straight, A., Kelly, K., Takuwa, Y., Sugimoto, N., Mitchison, T., and Bourne, H.R. (2003). Divergent signals and cytoskeletal assemblies regulate self-organizing polarity in neutrophils. Cell *114*, 201–214.
15. Zhao, M., Song, B., Pu, J., Wada, T., Reid, B., Tai, G., Wang, F., Guo, A., Walczysko, P., Gu, Y., et al. (2006). Electrical signals control wound healing through phosphatidylinositol-3-OH kinase-gamma and PTEN. Nature *442*, 457–460.
16. Rajnicek, A.M., Foubister, L.E., and McCaig, C.D. (2006). Growth cone steering by a physiological electric field requires dynamic microtubules, microfilaments and Rac-mediated filopodial asymmetry. J. Cell Sci. *119*, 1736–1745.
17. Kölsch, V., Charest, P.G., and Firtel, R.A. (2008). The regulation of cell motility and chemotaxis by phospholipid signaling. J. Cell Sci. *121*, 551–559.
18. Trollinger, D.R., Isseroff, R.R., and Nuccitelli, R. (2002). Calcium channel blockers inhibit galvanotaxis in human keratinocytes. J. Cell. Physiol. *193*, 1–9.

19. Lee, J., Ishihara, A., Oxford, G., Johnson, B., and Jacobson, K. (1999). Regulation of cell movement is mediated by stretch-activated calcium channels. Nature *400*, 382–386.
20. Euteneuer, U., and Schliwa, M. (1986). The function of microtubules in directional cell movement. Ann. N Y Acad. Sci. *466*, 867–886.
21. Minc, N., and Chang, F. (2010). Electrical control of cell polarization in the fission yeast Schizosaccharomyces pombe. Curr. Biol. *20*, 710–716.
22. Iglesias, P.A., and Devreotes, P.N. (2008). Navigating through models of chemotaxis. Curr. Opin. Cell Biol. *20*, 35–40.
23. Allen, G.M., Mogilner, A., and Theriot, J.A. (2013). Electrophoresis of cellular membrane components creates the directional cue guiding keratocyte galvanotaxis. Curr. Biol. Published online March 28, 2013. http://dx.doi.org/10.1016/j.cub.2013.02.047.
24. Houk, A.R., Jilkine, A., Mejean, C.O., Boltyanskiy, R., Dufresne, E.R., Angenent, S.B., Altschuler, S.J., Wu, L.F., and Weiner, O.D. (2012). Membrane tension maintains cell polarity by confining signals to the leading edge during neutrophil migration. Cell *148*, 175–188.
25. Wong, K., Pertz, O., Hahn, K., and Bourne, H. (2006). Neutrophil polarization: spatiotemporal dynamics of RhoA activity support a self-organizing mechanism. Proc. Natl. Acad. Sci. USA *103*, 3639–3644.
26. McLaughlin, S., and Poo, M.M. (1981). The role of electro-osmosis in the electric-field-induced movement of charged macromolecules on the surfaces of cells. Biophys. J. *34*, 85–93.

Current Biology, Volume *23*

Supplemental Information

Keratocyte Fragments and Cells Utilize Competing Pathways to Move in Opposite Directions in an Electric Field

Yaohui Sun, Hao Do, Jing Gao, Ren Zhao, Min Zhao, and Alex Mogilner

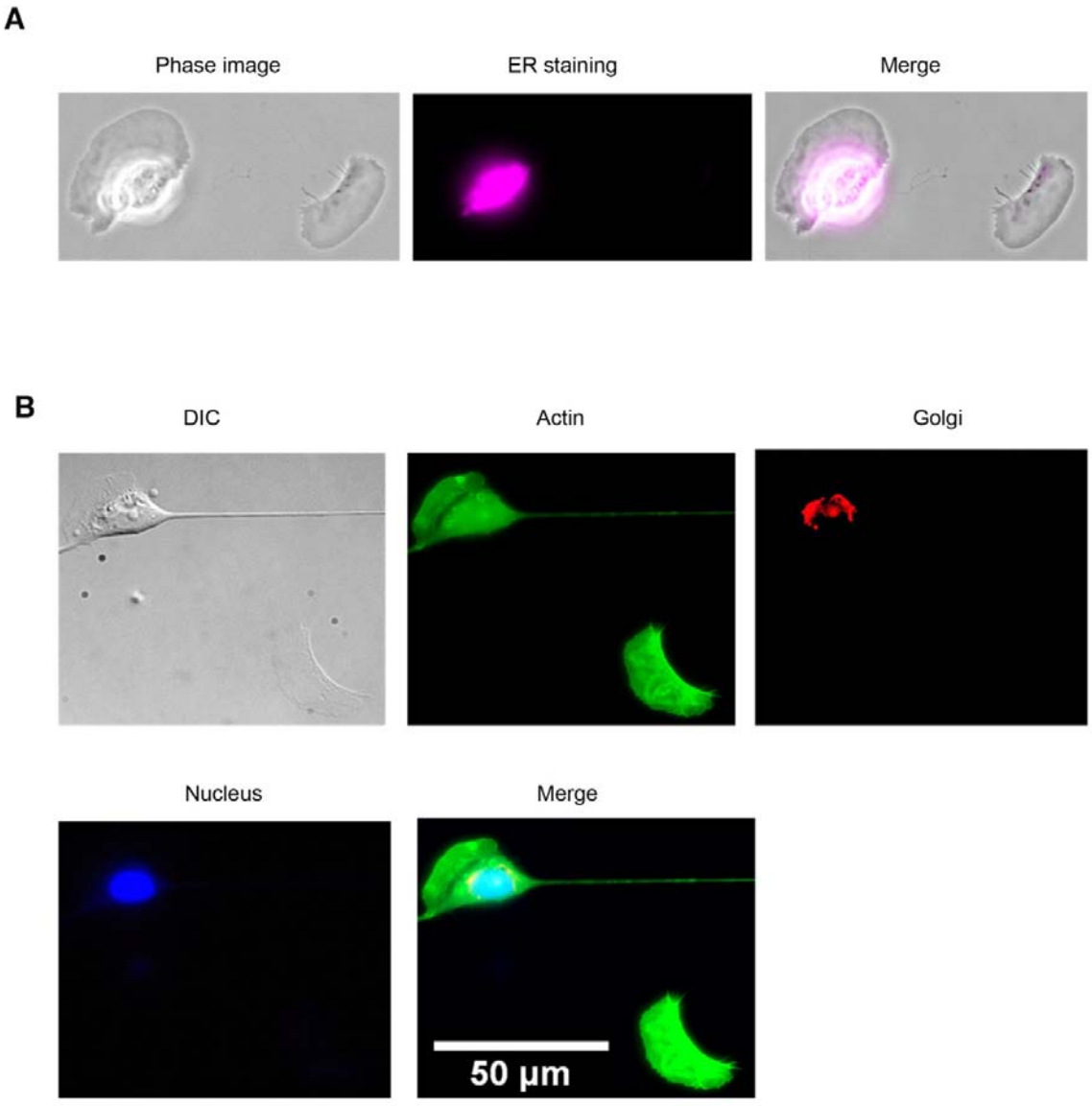

Figure S1. Fragments lack Nucleus, Endoplasmic Reticulum and Golgi, Related to Figure 3
(A) Images for keratocyte and fragment in phase contrast (left panel), with labeled ER (Middle panel in magenta) and merged (right panel). Note: there were fragments with no ER at all;

however, a number of fragments displayed some stain with the ER tracker that was much weaker than that displayed by the whole cells.
(B) Images for keratocyte and fragment in DIC (upper left panel), with labeled actin (green), Golgi (red), counterstained nuclei (blue) and merged (lower right panel). Scale bar equals 50 μm.

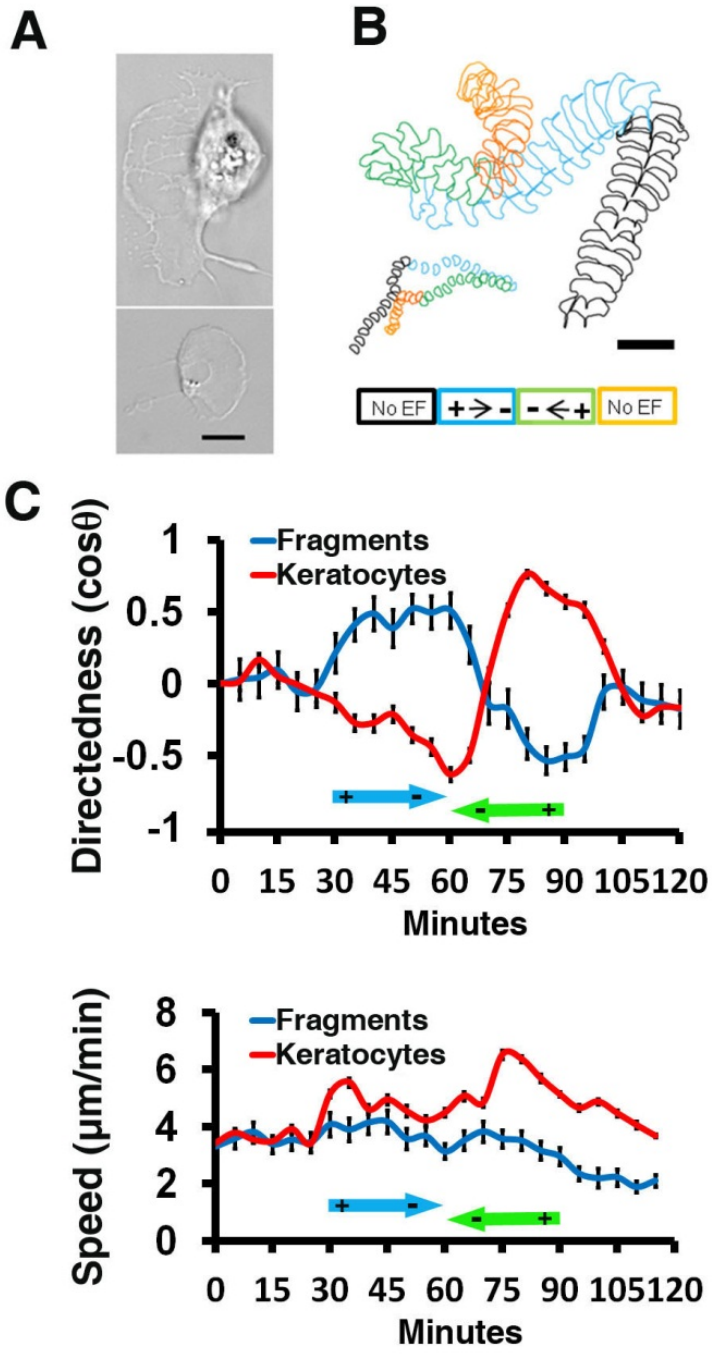

Figure S2. **Both cells and fragments respond rapidly to the EF direction switch, Related to Figure 1**

(A) DIC images of representative keratocyte (top panel) and fragment (bottom panel) generated with Staurosporin treatment. Scale bar equals 5 μm.

(B) Contour overlays of the cell and fragment shown in (A) during a 120 minute time course. EF polarity (4 V/cm) is color coded. Scale bar equals 50 μm.

(C) Directedness and trajectory speed of keratocytes (n = 13) and fragments (n = 32) as functions of time with 5 minute increments. EF polarity (4 V/cm) is color coded.

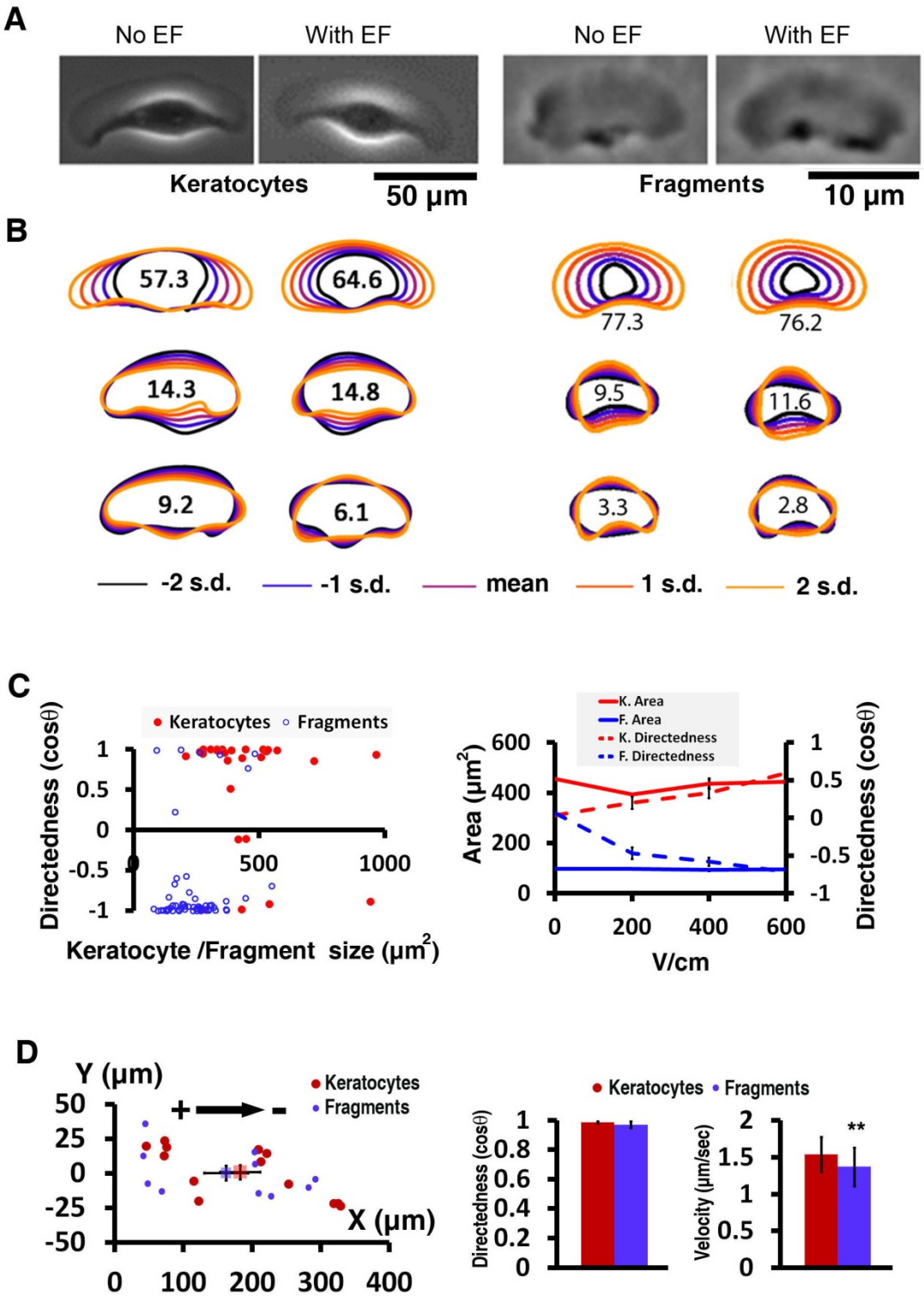

Figure S3. Galvanotaxis of cells and fragments is size- and shape-independent, Related to Figure 4

(A) Phase contrast images of representative keratocytes (left panels) and fragments (right panels) with and without EF exposure.

(B) Shapes of cells and fragments are not affected significantly by EF: Principal modes of shape variation of keratocytes (left panels) and fragments (right panels) with or without EF exposure, as determined by principal component analysis of aligned cell outlines. For each population of cells, the mean keratocyte/fragment shape and shapes one and two standard deviations from the mean are shown for each shape mode. The variation accounted for by each mode is indicated.
(C) Left: Scatter plots show directedness as a function of the size of keratocyte (red) and fragment (blue). The areas (μm^2) of keratocytes or fragments exposed to an EF of 6 V/cm for 30 minutes were measured and used for correlation analysis. Correlation coefficient is less than 0.2. Right: Directedness (dashed lines) of keratocyte cells and fragments is voltage dependent but size independent. No correlation between directedness and average area (solid lines) of keratocyte/fragment under different EF strength could be drawn.
(D) Electrophoretic properties of keratocyte (red, n = 13) and fragment (blue, n = 10). Scatter plot of the end point coordinates of keratocytes and fragments in suspension when exposed to an EF of 4 V/cm for 2 minutes (left panel). Squares represent the average values for each population; error bars indicate standard error of the mean. EF vector is marked by +/– and its orientation is indicated by arrow. Under EF strength of 4 V/cm, both keratocytes and fragments move with nearly maximal directionality to the cathode (middle panel). Fragments migrate slightly slower than keratocytes (right panel, **: $p < 0.01$).

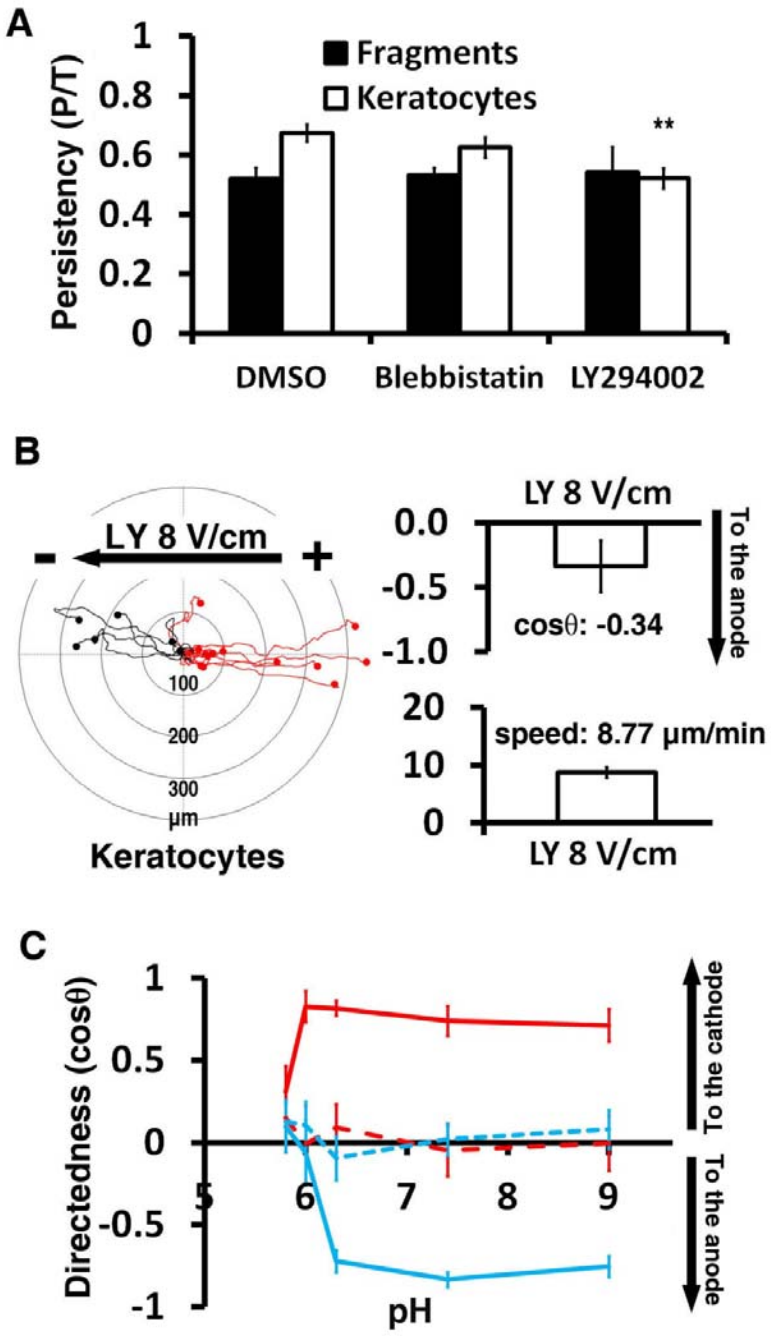

Figure S4. Effects of PI3K and myosin inhibition and pH level on cells' and fragments' persistency and directedness in EF, Related to Figure 2

(A) Keratocytes and fragments were treated with Blebbistatin (50 μM) or LY294002 (50 μM). Images were taken every 30 seconds. Migration persistency is calculated by displacement distance / trajectory distance after cells or fragments travelled for 30 minutes. Decreased migration persistency was observed in keratocytes but not fragments in the presence of PI3K inhibitor. ** ($p < 0.01$) indicates that the difference between DMSO and LY294002 is significant.

(B) Left: Trajectories of keratocytes in the presence of LY294002 when exposed to an EF of 8 V/cm. Total of 18 cells were traced. 12 were directed to the anode (red) while 6 to the cathode (black). Note that one cell originally migrating to the cathode underwent direction switching. Right: Quantification of directionality (top) and speed (bottom) of keratocytes (n=18) in the presence of LY294002 (50 μM). EF = 8 V/cm. Duration: 30 minutes.
(C) Directedness of keratocytes (red) and fragments (blue) in EF (solid lines) as functions of pH compared to the controls in the absence of an EF (dotted lines).

Table S1. Summary of directionality and speed of keratocytes and fragments exposed to EF under various conditions, Related to Figure 2

Condition/Voltage (V/cm)		Keratocytes			Fragments		
		N	Directedness (cosθ) Mean ± SE	Speed (μm/min) Mean ± SE	N	Directedness (cosθ) Mean ± SE	Speed (μm/min) Mean ± SE
	0.0	53	0.06 ± 0.05	6.16 ± 0.21	40	-0.13 ± 0.05	4.73 ± 0.21
	0.1	47	-0.01 ± 0.11	3.79 ± 0.24	47	-0.04 ± 0.11	5.32 ± 0.39
	0.2	47	0.18 ± 0.10	3.30 ± 0.21	60	0.12 ± 0.10	2.74 ± 0.23
	0.5	53	0.06 ± 0.09	5.78 ± 0.48	61	-0.28 ± 0.08	4.65 ± 0.29
	1.0	32	0.14 ± 0.08	5.71 ± 0.43	53	-0.22 ± 0.11	4.73 ± 0.34
	2.0	51	0.20 ± 0.08	7.16 ± 0.42	50	-0.47 ± 0.08	3.24 ± 0.17
	4.0	24	0.81 ± 0.07	8.26 ± 0.74	30	-0.65 ± 0.12	3.40 ± 0.56
	6.0	39	0.77 ± 0.05	7.03 ± 0.31	151	-0.59 ± 0.05	3.43 ± 0.13
DMSO	4.0	52	0.65 ± 0.06	11.11 ± 0.59	54	-0.66 ± 0.08	4.99 ± 0.42
LY294002	4.0	52	0.08 ± 0.11	5.62 ± 0.28	21	-0.45 ± 0.23	5.45 ± 0.75
Blebbistatin	4.0	51	0.82 ± 0.06	9.39 ± 0.39	57	-0.15 ± 0.11	7.60 ± 0.47
LY+BB	4.0	34	0.06 ± 0.13	7.58 ± 0.64	30	-0.14 ± 0.13	9.25 ± 0.89
Y27632	4.0	32	0.47 ± 0.11	5.39 ± 0.34	55	-0.22 ± 0.09	5.65 ± 0.25
CK-666	4.0	22	0.83 ± 0.07	4.84 ± 0.30	22	-0.23 ± 0.15	4.16 ± 0.26
EGTA	4.0	30	0.82 ± 0.03	3.87 ± 0.18	41	-0.10 ± 0.12	2.60 ± 0.15
Nocodazole	4.0	54	0.45 ± 0.10	9.73 ± 0.47	52	-0.42 ± 0.09	6.40 ± 0.35
pH 5.8	4.0	22	0.31 ± 0.16	0.01 ± 0.46	27	0.10 ± 0.13	0.01 ± 0.75
pH 6.0	4.0	21	0.83 ± 0.10	3.15 ± 0.22	17	-0.06 ± 0.20	3.08 ± 0.34
pH 6.3	4.0	30	0.82 ± 0.04	11.63 ± 0.54	30	-0.72 ± 0.07	8.23 ± 0.40
pH 7.4	4.0	27	0.74 ± 0.09	12.98 ± 1.14	44	-0.83 ± 0.04	8.25 ± 0.64
pH 9.0	4.0	16	0.71 ± 0.10	5.81 ± 0.39	34	-0.75 ± 0.06	5.49 ± 0.39

Data from a representative experiment.
Directedness is calculated as cosine angle between lines of displacement and electric field vector 30 minutes after the exposure. Positive: moving to cathode. Negative: moving to anode.
Drugs were applied as described in Experimental Procedures.
pH was adjusted as described in Experimental Procedures.

SUPPLEMENTAL EXPERIMENTAL PROCEDURES

The Institutional Animal Use and Care Committees of the University of California at Davis approved the animal procedures used in this study (protocol number is 16478), which were performed in accordance with NIH guidelines.

Keratocyte isolation and fragment induction: Scales were removed from the flanks of black skirt tetra *Gymnocorymbus ternetzi* and allowed to adhere to the bottom of a culture dish. The scales were covered by a glass 22-mm coverslip with a stainless steel nut on the top to hold the scales in position, and cultured at room temperature in Leibovitz's L-15 media (Gibco BRL), supplemented with 14.2 mM HEPES pH 7.4, 10% Fetal Bovine Serum (Invitrogen), and 1% antibiotic-antimycotic (Gibco BRL). Sheets of keratocytes that migrate off the scale after 24-48 hours were dissociated by a brief treatment with 0.25% Trypsin/0.02 EDTA solution (Invitrogen) in phosphate buffered saline (PBS). Isolated keratocytes were seeded in tissue culture dish and incubated at room temperature for 1-3 hours to allow attachment. Cell fragment formation was induced by 100 nM staurosporine (Sigma) in culture media at 35°C for 30 min with the lid half open. Cells and fragments are washed in normal media and allowed to recover for at least 10 min before observation on the microscope [1].

EF application and time-lapse recording: The electrotaxis experiments were carried out as previously described [2-4] in custom-made electrotaxis chambers (20 mm x 10 mm x 0.1 mm). The chambers were built over tissue culture treated dishes. These custom-made electrotaxis chambers with small cross-sectional area provided high resistance to current flow and minimized Joule heating during the experiment. To eliminate toxic products from the electrodes that might be harmful to cells, agar salt bridges made with 1% agar gel in Steinberg's salt solution were used to connect silver/silver chloride electrodes in beakers of Steinberg's salt solution to pools of excess medium at either side of the chamber.

Cell migration was recorded with a Zeiss Axiovert 40 with a Hamamatsu C4742-95 CCD digital camera (Hamamatsu Corporation) attached. Time-lapse experiments were performed using a SimplePCI 5.3 imaging system with a motorized X, Y, Z stage (BioPoint 2, Ludl Electronic Products Ltd.). Typically in each experiment, 4-6 fields under low magnification of 10x were chosen. Images were taken at 30 second intervals at room temperature. Each experiment lasted up to 2 hours. Drugs (all purchased from Sigma) were added in the medium in the following concentration: DMSO (0.1%), LY294002 (50 μM), Blebbistatin (50 μM), Y27632 (10 μM), EGTA (5 mM), Nocodazole (10 μM), CK-666 (100 μM). To adjust the pH in Leibowitz-15 media with 10% fetal bovine serum we titrate the media with 15 mM of appropriate buffers. For media with a pH of 5.8, 6.0, or 6.2, MES buffer was used. For media with a pH of 7.4, HEPES buffer was used. For media with a pH of 9, Tris buffer was used. [5]. In the case of electrophoretic experiment, keratocytes and fragments were released with trypsin/EDTA, washed once with normal medium and seeded in electrotaxis chamber. Time-lapse recording was processed immediately before cellular attachment to the surface.

Data processing and quantification: Time-lapse images were imported into ImageJ (http://rsbweb.nih.gov/ij). Tracks were marked by using the MtrackJ tool and plotted by using the Chemotaxis tool. Two parameters of cell migration were quantified: 1) Directedness, a

measurement to quantify how directionally cells migrated in response to EFs [6]. The angle that each cell moved with respect to the EF vector was measured and its cosine value was calculated as directedness [7]. If a cell moved perfectly along the field vector toward to cathode, the cosine of this angle would be 1; if the cell moved perpendicularly to the field vector the cosine of this angle would be 0; and -1 if the cell moved directly toward to anode. 2) Trajectory speed, which is used to define the migration rate, is the distance (in μm) traveled by the cell over sixty-second interval divided by this time interval (during this interval, cells and fragments turn little, so this measurement introduces but a small error). To measure the cell size, the initial two dimensional areas of keratocytes and fragments right before EF application were calculated in ImageJ.

Contour overlay and principal component analysis: Phase contrast images of keratocytes or fragments were converted into the binary images using custom written Matlab code (Script available upon request). Briefly, we used Matlab edge detection and a basic morphology function to outline the cells/fragments in the phase contrast image. We use the Otsu method [8] to erase the halo artifacts. If shape was still unsatisfactory, we then used the Lasso tool in Photoshop (Adobe) to manually extract the cell shape. Contours were extracted from the binary images and plotted in Celltool [9], an open source software, to simulate the motion of the cells/fragments over time. For principle component analysis, polygons were extracted from a large population of cell images and mutually aligned. Principal modes of shape variation were determined by principal component analysis of the population of polygonal cell outlines, and scaled in terms of the standard deviation of the population for each mode of variation, which was detailed previously [10].

Fluorescence labeling: Trypsinized cells were seeded in glass bottom plates. Fragments were induced with 100 nM Staurosporin for 30 minutes at 35^{o}C. Samples were fixed in 4% paraformaldehyde and permeabilized with 0.5% Triton X-100 in Phosphate buffered saline (PBS). All dyes were purchased from Invitrogen and used per manufacturer's instructions. The Golgi body was labeled with 10 μg/ml wheat germ agglutinin (WGA) conjugated with Alexa Fluor 594. Actin was stained with 5 μg/ml Phalloidin conjugated with Alexa Fluor 488 and the nucleus was stained with 2 μg/ml Hoechst 33342. The Endoplasmic Reticulum (ER) of live cells was labeled with 1 μM ER-Tracker Red (glibenclamide BODIPY TR). Staining was performed in Hank's Balanced Salt Solution (HBSS) with calcium and magnesium (116.5mM NaCl, 5.4mM KCl, 0.25mM Na2HPO4, 0.44mM KH2PO4, 1.3mM CaCl2, 1mM MgSO4, 4.2mM NaHCO3). Cells were incubated at room temperature with the staining buffer for 30 min. After washing with fresh medium, fragments were induced by staurosporine treatment. Images were taken in a Zeiss Axio-Observer inverted microscope equipped with a CoolSnap HQ2 CCD camera (Photometrics) using a 63x objective (NA=1.4) and 1.6 optovar.

Statistics: All experiments were repeated and produced similar results. In most cases a representative experiment is shown, unless stated otherwise. Data are presented as means ± standard error. In order to conclude the size dependency a correlation coefficient corresponding to the directedness were calculated. To compare group differences (EF *vs* no EF or drug treatment *vs* no treatment) either chi-squared test or paired/unpaired, two-tailed Student's *t*-test were used. A *P* value less than 0.05 is considered as significant.

Supplemental References

1. Ofer, N., Mogilner, A., and Keren, K. (2011). Actin disassembly clock determines shape and speed of lamellipodial fragments. Proceedings of the National Academy of Sciences of the United States of America *108*, 20394-20399.
2. Zhao, M., Agius-Fernandez, A., Forrester, J.V., and McCaig, C.D. (1996). Directed migration of corneal epithelial sheets in physiological electric fields. Invest Ophthalmol Vis Sci *37*, 2548-2558.
3. Song, B., Gu, Y., Pu, J., Reid, B., Zhao, Z., and Zhao, M. (2007). Application of direct current electric fields to cells and tissues in vitro and modulation of wound electric field in vivo. Nat Protoc *2*, 1479-1489.
4. Sun, Y.H., Reid, B., Fontaine, J.H., Miller, L.A., Hyde, D.M., Mogilner, A., and Zhao, M. (2011). Airway Epithelial Wounds in Rhesus Monkey Generate Ionic Currents That Guide Cell Migration to Promote Healing. J Appl Physiol.
5. Allen, e.a. (2012). Electrophoresis of cellular membrane components creates the directional cue guiding galvanotaxis.
6. Tai, G., Reid, B., Cao, L., and Zhao, M. (2009). Electrotaxis and wound healing: experimental methods to study electric fields as a directional signal for cell migration. Methods Mol Biol *571*, 77-97.
7. Gruler, H., and Nuccitelli, R. (1991). Neural crest cell galvanotaxis: new data and a novel approach to the analysis of both galvanotaxis and chemotaxis. Cell Motil Cytoskeleton *19*, 121-133.
8. Otsu, N. (1979). A threshold selection method from gray-level histograms. IEEE Transactions on Systems, Man and Cybernetics *9*, 62-66.
9. Pincus, Z., and Theriot, J.A. (2007). Comparison of quantitative methods for cell-shape analysis. J Microsc *227*, 140-156.
10. Barnhart, E.L., Lee, K.C., Keren, K., Mogilner, A., and Theriot, J.A. (2011). An adhesion-dependent switch between mechanisms that determine motile cell shape. PLoS biology *9*, e1001059.